Measuring stress field without constitutive equation

Marie Dalémat, Michel Coret, Adrien Leygue, Erwan Verron

Measuring stress field without constitutive equation

Marie Dalémat, Michel Coret, Adrien Leygue & Erwan Verron

June 14, 2019

Abstract

The present paper proposes a coupled experimental-numerical protocol to measure heterogeneous stress fields in a model-free framework. This work contributes to developing the emerging realm of mechanics without constitutive equation. In fact, until now these types of simulations have been missing database of real and rich material behaviour. The technique consists in coupling Digital Image Correlation (DIC) measurements and the Data Driven Identification (DDI) algorithm, recently developed by Leygue *et al.*(*Data-based derivation of material response*. Computer Methods in Applied Mechanics and Engineering **331**, 184–196 (2018)). This algorithm identifies the mechanical response of a material, *i.e.* stress-strain data, without postulating any constitutive equation, but with the help of a large database of displacement fields and loading conditions. The only governing equation used in this algorithm is the mechanical equilibrium. The bias induced by the choice and the calibration of a constitutive model is thus removed. In the above-mentioned paper, the relevance of the method has been demonstrated with synthetic data issued from finite element computations. Here, its efficiency is assessed with "real" experimental data.

A multi-perforated elastomer membrane is uniaxially stretched in large strain. Practical challenges are addressed when using the DDI algorithm, especially those due to unmeasured data during experiments. Easy-to-implement solutions are proposed and the DDI technique is successfully applied: heterogeneous stress fields are computed from real data. Considering that the material is elastic, its strain energy density is then measured. Good agreement with standard uniaxial tensile experimental results validates the approach on real data.

Highlights

- Data Driven Identification technique is applied to measured displacements and forces
- Experimental stress field is determined without presupposing constitutive equation
- Practical solutions to use Digital Image Correlation raw data are provided
- The technique is applied to a perforated elastomer sheet under large strain

1 Introduction

The formulation of deformable mechanical problems involve two types of governing equations. On the one side, the equilibrium (or motion) equations and compatibility conditions (displacement-strain relationships) are uncertainty free; on the other side the constitutive equations which reflect the material response are to use with caution. First, the choice of a constitutive model is rendered difficult by the large number of available models (see for example [1] for hyperelasticity). Second, the model parameters must be determined thanks to experimental data, which are by nature restricted to specific deformation states. Practically, a constitutive equation can be seen as the way *(i)* to produce an unnoisy continuous response of a given material from simple mechanical tests, *(ii)* to interpolate the response between measured data points, but more importantly *(iii)* to extrapolate to other deformation states, larger strain and/or dimensions (from 1D to 2D or 3D). Obviously such extrapolation is difficult to validate experimentally and may lead to inaccurate numerical results.

The continuous improvement of full-field measurement techniques such as Digital Image Correlation (DIC), presented for example in [2], allows the identification of model parameters considering non-standard tests, e.g. experiments with complex geometry and/or loading conditions that involves inhomogeneous fields. Among others, we can mention the Virtual Field Method, the Equilibrium Gap Method, the Constitutive Equation Gap Method, the Reciprocity Gap Method and Finite Element Model Updating; for overviews on theses approaches, the interested reader can refer to [3] and [4].

Plus, thanks to the development of "Data Driven" techniques (also referred to as Machine Learning or data mining in various fields, e.g. science, marketing... [5]), new techniques are proposed for materials response in order to assist engineers in both identification and simulation processes. It is to note that unlike Data mining techniques in other fields, physical considerations on material response, e.g. isotropy or other invariances, can greatly help the dedicated solvers [6]. Neural networks are used to determine the material parameters of hyperelastic models [7] and of viscoplastic ones [8]; but also to improve finite element procedures [9]. Manifold learning approaches are considered as well: for example to identify material response using the imprint shapes of indentation tests [10] and to improve elastodynamic simulations [11]. Eventually, the robust identification of the model parameters remains a complex task. Finally, it is sometimes argued that the constitutive equation paradigm has reached a limit; this is the reason why some authors propose to overcome the difficult choice of a constitutive equation by replacing it by the identification of the material response without any underlying constitutive equations. In this different way of thinking, the cornerstone is to develop strain-stress databases filled with sufficiently "rich" and "smart" information for simulation tools. Thus, material response must be gathered for a large set of different loading conditions, for which stress is usually difficult to measure. For example, for small strain elastoplasticity, Réthoré *et al.* measure stress and strain fields from

equilibrium equations and DIC measurements by introducing a specific decomposition of the measured strain field and computing the stress fields [12]. Also, Seghir and Pierron demonstrate that stress fields can be computed considering DIC measurements during dynamic experiments [13]: for samples submitted to ultrasonic vibrations, they measure both displacement and acceleration fields with an ultra-high speed camera; then the stress field is calculated by considering the motion equation without any force measurement neither constitutive equation. Finally, for hyperelasticity, Latorre *et al.* propose the concept of *What-You-Prescribed-is-What-You-Get (WYPiWYG)* that consists in replacing the standard strain energy density function with model-free splines [14]. This technique is used with real data; nevertheless it is produced by basic tests where stress fields are easily measured.

In the present paper, a novel method of identification is considered: the "Data-Driven Identification" (DDI) algorithm [15]. It is based on the recent "Data Driven Computational Mechanics" (DDCM) paradigm: bypassing the constitutive equations in mechanical problem formulation [16]. Its originality lies in the absence of an explicit constitutive equation in the governing equations: during finite element computations, the classical constitutive equation is replaced by a large stress-strain database. This theory was first introduced by Ortiz *et al.* [16] and completed for noise dealing [17], large strain [18] and dynamic problems [19]. Roughly speaking, in the DDCM framework the mechanical response of a structure is directly computed considering a large database of "material states", these material states being strain-stress couples that sample the material response. The corresponding algorithm consists in the minimization of the distance between the "mechanical states", *i.e.* the strain-stress couples to calculate (in each finite element of the mesh for instance) and the material states database, under the constraints of satisfying both equilibrium equations and compatibility conditions. Slightly different formulations of this solver have been proposed [20, 21].

The Data Driven Identification method modifies the DDCM technique for identification of stress fields: for complex experiments, the heterogeneous stress fields are computed without constitutive equation. The success of the method is closely related to the availability of a large database of mechanical problems, *i.e.* sample geometry and loading conditions and their corresponding displacement fields. This approach has been validated only with synthetic data for truss structures and for small-strain (non linear) elasticity [15]. Here, we aim at validating the DDI approach with real experimental data. Practically, it consists in computing stress fields from displacement fields measured by DIC during the uniaxial extension of a perforated elastomer sheet. In the following, the DDI algorithm is first briefly recalled. Then, the experimental procedure is described; the emphasis is laid on the practical challenges induced by real data as compared to synthetic data: the mechanical problem has to be reformulated at the boundaries due to the unavailability of a few data (close to the grips or holes and in noise affected areas). Once these difficulties overcome, results consists in "measured" heterogeneous stress fields on the membrane surface. The relevance of these results is validated by comparison with standard uniaxial tensile experiments and the experimental derivation of the

strain energy density of the material is discussed.

2 Brief recall of the Data-Driven Identification method

The DDI method consists in computing heterogeneous stress fields without constitutive equation, using a large database of measured displacement fields. In [15], the derivation is proposed for small strain (non linear) elasticity. In the following, only the basics of the method are recalled.

2.1 Inputs and outputs

We consider a set of mechanical problems defined by its geometry through a meshed 2D-structure and a given set of loading conditions (denoted by the superscript $\cdot^Y$). Once the corresponding experiment being conducted, the following quantities are assumed to be available:

- (I-1) the nodal displacements $\mathbf{u}_j^Y$, j being the node number,
- (I-2) the matrix $\mathbf{B}_{ej}^Y$ that encodes both geometry and connectivity, e being the quadrature point number. Then, the strain field at point e is defined by (for small strain):

$$\boldsymbol{\varepsilon}_e^Y = \sum_j \mathbf{B}_{ej}^Y \cdot \mathbf{u}_j^Y, \tag{1}$$

- (I-3) the nodal forces $\mathbf{f}_j^Y$, which are null in the bulk (interior of the mesh) and known on the boundaries;

  These quantities are the inputs of the DDI algorithm. The following two are the intrinsic parameters of the methods:

- (In-1) the size N^* of the (stress-strain) database that samples the material response,
- (In-2) the norm $\mathbb{C}$ that defines the distance between two points in the stress-strain space.

After convergence, the DDI algorithm computes the following outputs:

- (O-1) for each problem Y, the stress field $\boldsymbol{\sigma}_e^Y$ that satisfies the equilibrium equations at each integration point e:

$$\sum_e w_e^Y \mathbf{B}_{ej}^Y \cdot \boldsymbol{\sigma}_e^Y = \mathbf{f}_j^Y \quad \forall Y, j, \tag{2}$$

  where w_e^Y is the integration weight of point e. The pair composed by the strain and stress at a given point of the mesh $(\boldsymbol{\varepsilon}_e^Y, \boldsymbol{\sigma}_e^Y)$ is referred to as a *mechanical state* because it is mechanically admissible, *i.e.* it fulfills both compatibility and equilibrium equations,

- (O-2) the database of *material states* $(\varepsilon_i^*, \sigma_i^*)$ that maps the mechanical response of the material. The total number of material states is N^*; the distance to mechanical states is evaluated thanks to the " norm $\mathbb{C}$", which is chosen in an energetic manner, $\mathbb{C}$ being a fourth-order positive definite pseudo-stiffness tensor:

$$||(\varepsilon, \sigma)||_{\mathbb{C}}^2 = \frac{1}{2}(\varepsilon : \mathbb{C} : \varepsilon + \sigma : \mathbb{C}^{-1} : \sigma). \tag{3}$$

2.2 Some details on the DDI method

For a given number of mechanical problems, the algorithm aims at finding the material states that are the closest to the mechanical states, the latest being half known (strain) and half unknown (stress) but constrained by equilibrium equations. Mathematically, it reduces to the following constrained minimization problem:

$$\text{solution} = \arg \min_{\sigma_e^Y, \varepsilon_{e^Y}^*, \sigma_{e^Y}^*} \mathscr{E}(\sigma_e^Y, \varepsilon_{e^Y}^*, \sigma_{e^Y}^*) \tag{4}$$

where

$$\mathscr{E}(\sigma_e^Y, \varepsilon_{e^Y}^*, \sigma_{e^Y}^*) = \sum_Y \sum_e w_e^Y \, ||(\varepsilon_e^Y - \varepsilon_{e^Y}^*, \sigma_e^Y - \sigma_{e^Y}^*)||_{\mathbb{C}}^2, \tag{5}$$

under the constraints

$$\begin{cases} \text{of respecting equilibrium equations (2),} \\ \text{that the material state } (\varepsilon_{e^Y}^*, \sigma_{e^Y}^*) \text{ associated to the element } e^Y \text{ belong to the database } (\varepsilon_i^*, \sigma_i^*)_{i=1}^{N^*}. \end{cases}$$

Practically,

- The initial step computes the material states by the *k-means* algorithm [22] over the measured mechanical strain and the stresses are set to zero.
- Then, the procedure iteratively
  1. computes the material stress to "recenter" them in the cloud formed by the mechanical states (according to the norm $\mathbb{C}$),
  2. updates the mechanical stresses to be at equilibrium and as close as possible to the material stress,
  3. computes the mapping between mechanical and materials states,
  4. updates the material strain,

  until convergence.

In [15], the validity of the DDI scheme has been assessed thanks to synthetic data.

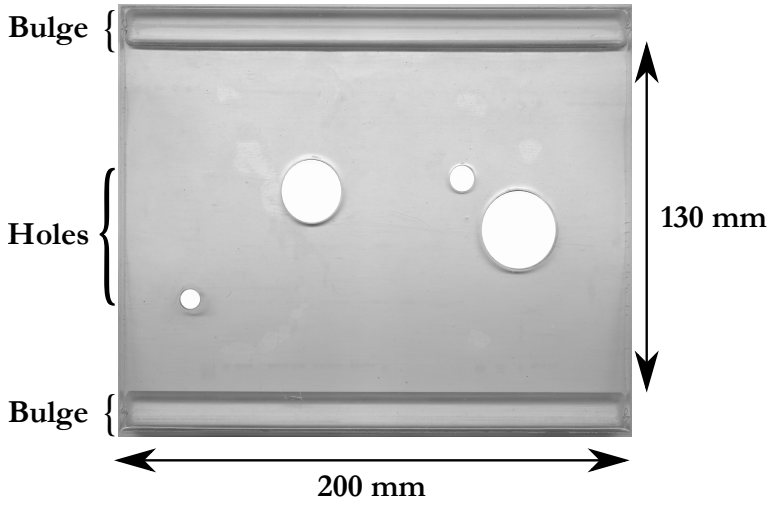

Figure 1: Silicone membrane, with bulges and holes. Thickness is about 3.7 mm.

3 Application of the DDI method to real data

In the present work, the relevance of the DDI algorithm is demonstrated with real experimental data. For this first "real-life" application, we consider the general context of large strain quasi-static elasticity thanks to the deformation of planar elastomer membranes. First, the experimental procedure is presented; then it is shown that the extension of the previous algorithm to large strain is straightforward. Finally, the main challenges of the application to real data are detailed: they concern the practical difficulties encountered, especially the incompleteness of measurements.

3.1 Experimental procedure

Material and samples The elastomer is an unfilled silicone elastomer Bluesil^{TM}RTV 141; it has been chosen because it does not exhibit any Mullins effect and then it can be considered purely elastic [23]. The strain at break, measured with standard uniaxial tensile test, is about 100%. Moreover, the material is assumed homogeneous, isotropic and incompressible.

Samples consist in thin rectangular sheets with bulges to fit the grips of the tensile machine; they are cured in an oven accordingly to the technical prescriptions. Once vulcanized, the membrane is perforated with hollow punches. The geometry of the sample is shown in Figure 1. Curing being performed in an open mould, sheets thickness is not prescribed but simply measured afterwards: 3.7 mm $\pm$ 0.7mm.

The plane stress assumption is adopted. Coupling it with the incompressibility hypothesis allows the reduction of measurements to planar components: if one

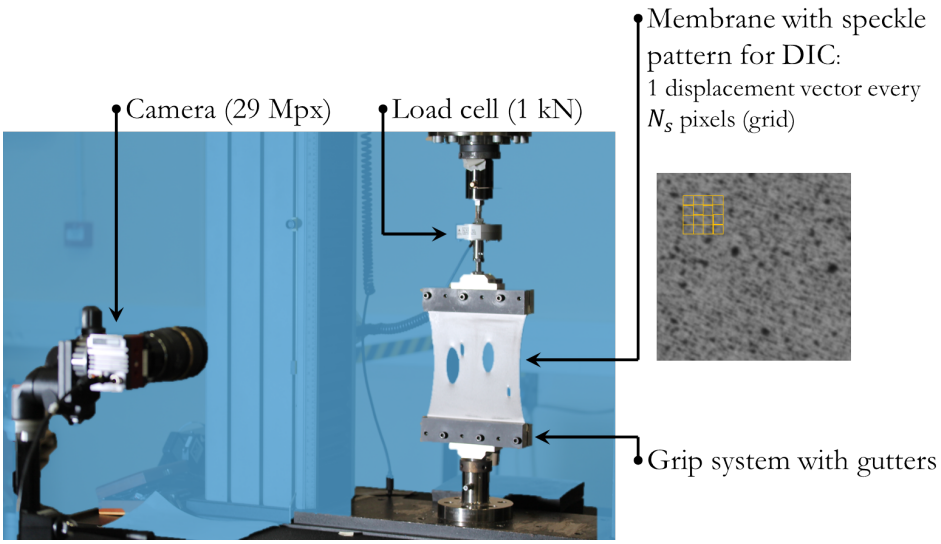

Figure 2: Experimental set-up: displacements are gathered with camera and DIC and force measurements with the load cell.

denotes 3 the thickness direction, the stress components $(\sigma_{i3})_{i=1,2,3}$ and the strain components $(\varepsilon_{i3})_{i=1,2}$ are null; and ε_{33} can be computed from in-plane quantities.

Experimental apparatus: loading conditions and measurements The experimental set-up is presented in Figure 2. The uniaxial tensile experiments are conducted with an Instron 3369 electromechanical tensile machine. A specific grip system holds the membrane by clamping the bulges. The loading speed is set to 12 mm/min which corresponds to an overall strain rate of about $1.5{\cdot}10^{-3}$ s^{-1} such that experiments can be considered as quasi-static.

The loading force is measured with a force cell. Kinematics are measured thanks to the DIC technique:

- a speckle pattern is applied (by spraying) on the surface of samples (that gives an approximate feature size of 10px),
- a 29 Mpx camera with a 100 mm-focal length lens (the camera is a AlliedVision GT 6600, with an image resolution of 6576 $\times$ 4384; the lens is a Zeiss makro-planar T* 2/100), is positionned at a stand-off distance $Z \approx 1$ m,
- and an appropriate lighting system is used.

Images are recorded and the displacement field is computed with the commercial software VIC-2D$^{\text{TM}}$(Correlated Solutions). The estimated out-of-plane motion (due to sample thinning) is about $\Delta Z = 0.3$ mm in average over the sample at the last increment, which gives an in-plane strain error of $\Delta Z/Z \approx 0.03\%$ according to [24]. The use of 2D-DIC rather than stereo-DIC is justified.

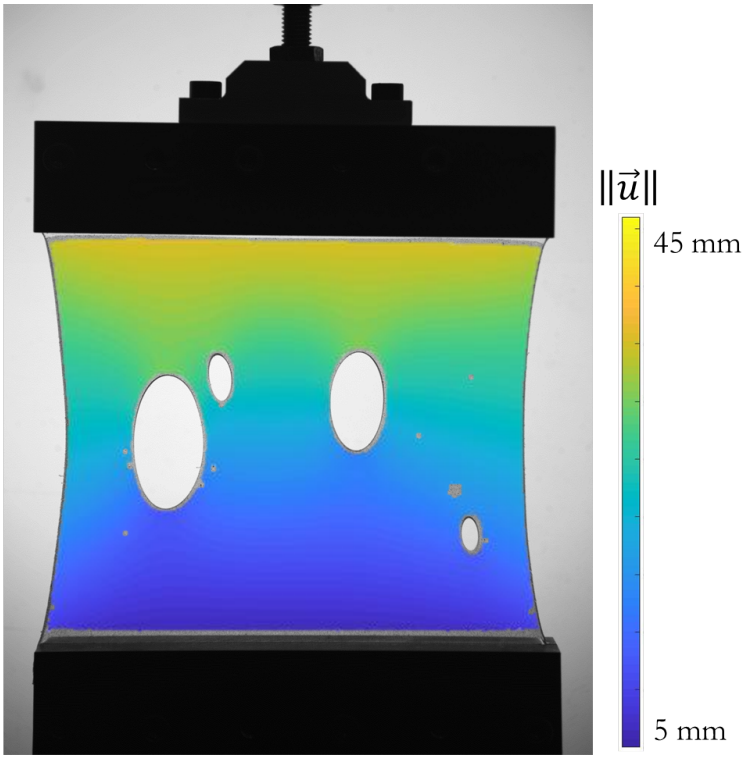

Figure 3: Example of a displacement field obtained with DIC at the last increment of the loading path.

Pictures are recorded every 1.5 s which corresponds to a reasonable engineering strain increment between 2 pictures. The acquisition time of the camera is chosen accordingly to satisfy both correct lighting and no significant change of grey level for one pixel (due to sample motion) during the acquisition. The equivalent pixel size is about 65 µm. The DIC experiments are carried out following the guidelines proposed in [25]. An example of recorded a displacement field is presented in Figure 3.

Concerning the order of magnitude of strain, the last loading increment corresponds to about 35% in terms of average engineering strain globally and 100% in terms of local engineering strain. Finally, in order to relate the measurements to the theoretical derivation of Section 2, the different mechanical problems denoted by the superscript Y correspond to the deformation of the samples subjected to different stretching increments. For each of them, the displacement field $\mathbf{u}_j^Y$ is measured with respect to the undeformed configuration.

3.2 Extension of the DDI algorithm to large strain

In order to adapt the DDI method to elastomer, Eqs (1)-(3) must be extended to large strain. For the sake of simplicity, the continuous formulation is chosen in this section, even though the discretised (Finite Element) form of the equations is used in the rest of the paper. Concerning the stress, we adopt an Eulerian description of the problem such that the Cauchy (true) stress σ can be retained. Nevertheless, the corresponding strain tensor must be adapted, the linearized strain tensor ε being not relevant to large strain. Following [26], we adopt the Hencky (true) strain tensor as the natural extension of ε to Eulerian large strain formulation. Considering the deformation gradient $\mathbf{F}$ and the left Cauchy-Green strain tensor $\mathbf{b} = \mathbf{F}\mathbf{F}^T$, the Hencky strain tensor is defined by:

$$\ln \mathbf{v} = \frac{1}{2} \ln \mathbf{b}, \tag{6}$$

where $\mathbf{v}$ is the (left) pure stretch tensor issued from the polar decomposition of the deformation gradient $\mathbf{F} = \mathbf{v}\mathbf{R}$. Then, the DDI algorithm is straightforwardly extended to large strain by replacing the linearized strain tensor by the Hencky strain tensor in all the previous equations. As an example, the norm in the stress-strain space Eq. (3) becomes:

$$||(\ln \mathbf{v}, \sigma)||^2_{\mathbb{C}} = \frac{1}{2}(\ln \mathbf{v} : \mathbb{C} : \ln \mathbf{v} + \sigma : \mathbb{C}^{-1} : \sigma). \tag{7}$$

The original method uses (ε, σ) and here is introduced the large strain extension. To deal with path-dependency (e.g. plasticity) problems, it might be possible to choose a richer phase space as in [27] or [28].

3.3 Practical challenges when applying the DDI method to "real" data

Application of DDI to real data faces two challenges that are closely related with the discrepancy between the real problem and the theoretical one. It is not possible to obtain mechanical states (strain and stress) at each element because of *(i)* the incompleteness of measured kinematic fields and *(ii)* the unavailability of nodal forces but of a unique net force measured through the load cell. In the following, we propose methods to handle these challenges by completing (wisely) the missing mechanical knowledge. These methods are not unique, but our proposals are easily implementable and they are validated on synthetic data in [29].

First, the theoretical boundary conditions of the problem must be recalled; they are sketched in Figure 4a. Let us denote Ω the bulk of matter where equilibrium Eq. (2) applies simply with $\mathbf{f}_j = \mathbf{0}$ (no volume force). The different boundaries are:

- the top boundary Γ_{T} where the load cell gives information. In a perfect (synthetic) case, the equilibrium equation is applied to each node (with nodal forces $\mathbf{f}_j$),

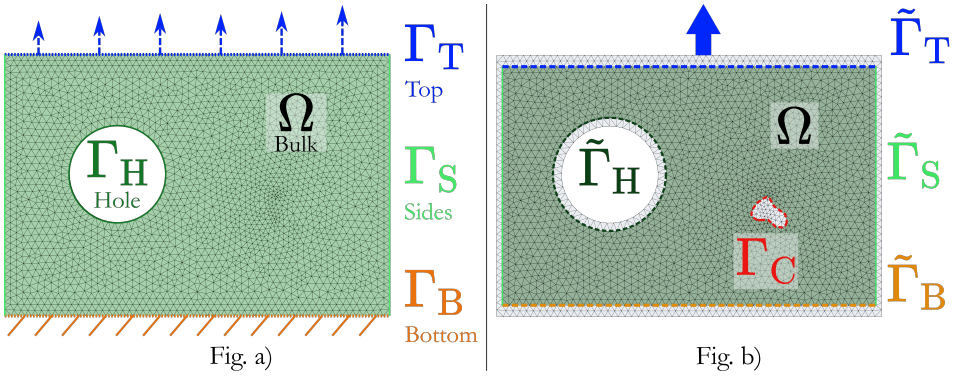

Figure 4: Fig. a) Theorethical boundaries of the mechanical problem of a perforated membrane under traction. Fig. b) Real boundaries after DIC (incompleteness is due to inaccurate edge selection and clusters of missing data).

- the bottom boundary Γ_B where no information is gathered, except displacements,
- the lateral sides of the membrane Γ_S. In the perfect case, they correspond to free edges where the mechanical equilibrium is easily assessed,
- the hole edges Γ_H for which free edge conditions apply.

3.3.1 Challenge *(i)*: incompleteness of measured kinematic fields

Reasons of incompleteness The incomplete nature of the measured kinematical fields is a classical issue when using DIC [30]. This full-field measurement technique is based on a local optimization method that consists in computing the displacement vector $\mathbf{u}$ which maximizes the correlation between an initial f and a deformed picture g (in grey level), in every subsets defined by few pixels. These subsets are forming the so-called Region Of Interest (ROI) and the correlation is evaluated at each pixel p to find $\mathbf{u}$, such that:

$$\mathbf{u} = \arg\min \sum_{p \in \mathrm{ROI}} [f(\mathbf{x}_p) - g(\mathbf{x}_p + \mathbf{u}(x_p))]^2, \tag{8}$$

where $\mathbf{x}_p$ is the position of the pixel p in the initial picture. Numerically, $\mathbf{u}$ can be approximated thanks to shape functions as in the Finite Element Method (for example see [31]) but non-parametrical approaches are also developed as in VIC-2D$^{\mathrm{TM}}$(the software considered here). In this software, each subset (of N_b^2 pixels) furnishes one displacement vector; but an overlap of the subsets is possible (N_s is the number of pixels between two subsets). In our case, it leads to one displacement vector $\mathbf{u}$ every $N_s = 7$ pixels, based on the computation in a $N_b^2 = 27^2$-pixel subset (chosen according to both noise and resolution). This naturally forms a structured

meshed in which nodal displacements are known every 7 pixels. Using a standard Finite Element approximation, the matrix $\mathbf{B}_{ej}^{Y}$ that encodes both geometry and connectivity for the mechanical problem Y, *i.e.* one deformed image, can be easily computed.

In VIC-2D^{TM}, the accuracy of measurements is controlled by choosing some threshold values above which data are removed. In particular, the "consistency error" checks the back-prediction between neighbour images. It consists in recomputing the supposed initial image from one deformed state image with the inverse displacement fields computed and in checking if the reconstructed initial image and the true initial image are close or not. Moreover, due to measurement noise and/or to large displacement between two successive images, there are some areas in which no displacement is given by the software. Therefore, some data are missing from the measured displacement field.

Definition of new boundaries When comparing with the theoritical problem shown in Figure 4a, it can be noticed that new boundaries have to be defined for the real problem. They are shown in Fig. 4b :

- First, due to *inaccurate edge selection* during the definition of the ROI (that is manually selected and constrained through N_s), there are some missing zones (and thus nodes) in the neighbourhood of the "true" boundaries: near free surfaces such as holes and sample borders and close to the grips. Thus, it leads to the definition of new boundaries that are close to the theoretical ones and denoted $\tilde{\Gamma}_{\mathrm{H}}$ for hole edges, $\tilde{\Gamma}_{\mathrm{S}}$ for the sides and $\tilde{\Gamma}_{\mathrm{T}}$ for top and $\tilde{\Gamma}_{\mathrm{B}}$ for bottom clamped lines.

- Second, after the DIC process, some data are removed if the consistency error is too large. The corresponding areas are small if displacements of surrounding nodes are well-measured (*isolated missing data*) or they can spread over few pixels (*cluster of missing data*). In the first case, the missing displacement value is interpolated from surrounding nodes. In the latter case, the mechanical states cannot be defined because the strain cannot be measured. This leads to the creation of new boundaries denoted Γ_{C} for each cluster of missing data.

3.3.2 Challenge *(ii)*: unavailability of all nodal forces

Practically, it is not possible to access nodal forces that apply on the top clamped line Γ_{T} (or $\tilde{\Gamma}_{\mathrm{T}}$): only the total net force F_{cell}^{Y} is measured by the load cell. Therefore, evaluating directly Eq. (2) is only possible in the bulk and at free edges where the force is respectively null and null along the normal direction. In our problem, the true free edges are not exactly known as explained in Section 3.3.1. Nevertheless, the side boundaries $\tilde{\Gamma}_{\mathrm{S}}$ can be reasonnably considered as free edges. This is not the case for the hole edges, for which this hypothesis would imply a large error; it has

been proven with synthetic data in [29] and not recalled here. A practical solution is proposed in the next section.

3.3.3 Completion with mechanical considerations

To summarize, the real problem has been deteriorated compared to the theoretical one, due to the incompleteness of measured kinematic fields (inaccurate edge selection and clusters of missing data) combined with the unavailability of a complete force information. This implies some missing strain or stress and thus impacts the whole mechanical state concerned.

Until then, it has been shown that getting the full mechanical state of the bulk Ω and of the sides $\tilde{\Gamma}_{\mathrm{S}}$ is possible through the measured strain and the computed stress with:

$$\sum_e w_e^Y \mathbf{B}_{ej}^Y \cdot \boldsymbol{\sigma}_e^Y = \mathbf{0} \quad \text{for} j \in \tilde{\Gamma}_{\mathrm{FE}} \cup \Omega. \tag{9}$$

Note that the free edges assumption is a particular case of the general equilibrium equation: equation $\boldsymbol{\sigma} \cdot \mathbf{n} = 0$, with the normal vector $\mathbf{n}$, is deductible from the specific geometry of an edge.

Therefore, some completion of the mechanical state is proposed thanks to some mechanical considerations:

- The load cell information has no contribution in the algorithm yet. Thus, our belief is that the only way to properly introduce it in the equilibrium equation is to consider that the net force is the sum of non-zero nodal forces $\mathbf{f}_j^Y$ which exerts on $\tilde{\Gamma}_{\mathrm{T}}$ in the loading direction $\mathbf{n}_{\mathrm{cell}}$, or so:

$$\sum_{j \in \tilde{\Gamma}_{\mathrm{T}}} \mathbf{f}_j^Y \cdot \mathbf{n}_{\mathrm{cell}} = F_{\mathrm{cell}}^Y. \tag{10}$$

  Thus, the balance equation on the top boundary is replaced by the force balance in the $\mathbf{n}_{\mathrm{cell}}$ direction:

$$\sum_{j \in \tilde{\Gamma}_{\mathrm{T}}} \sum_e w_e^Y \mathbf{B}_{ej}^Y \cdot \boldsymbol{\sigma}_e^Y \cdot \mathbf{n}_{\mathrm{cell}} = F_{\mathrm{cell}}^Y \qquad \forall Y. \tag{11}$$

  Note that we directly consider $\tilde{\Gamma}_{\mathrm{T}}$ instead of Γ_{T}. This approach is less constraining than evenly distributing the net force on the boundary.

- A cluster of missing data, denoted Ω_{C}, cannot be considered in the mechanical problem because no information has been gathered with DIC. We consider the surrounding nodes in which the displacements hava been measured and we denote Γ_{C} the boundary they form. The domain Ω_{C} is not considered in the problem but should be: in Ω_{C}, the matter is mechanically balanced. The equilibrium equations over $\Omega_{\mathrm{C}} \bigcup \Gamma_{\mathrm{C}}$ are written and summed. Their collapse in Ω_{C} gives a residual expression of the equilibrium on Γ_{C}:

$$\sum_{j \in \Gamma_{\mathrm{C}}} \sum_e w_e^Y \mathbf{B}_{ej}^Y \cdot \boldsymbol{\sigma}_e^Y = \mathbf{0}. \tag{12}$$

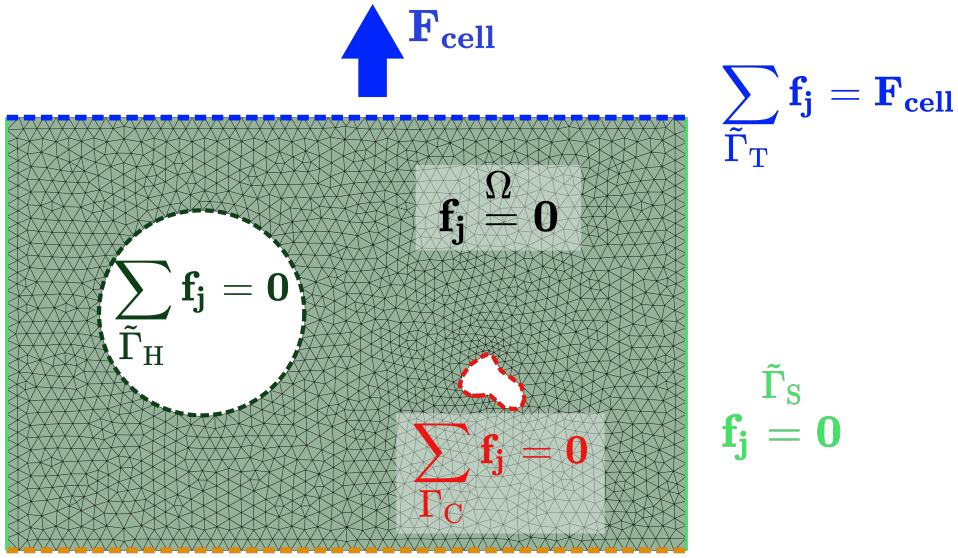

Figure 5: Practical challenges when using the DDI algorithm and our proposals to add mechanical considerations.

This condition represents the overall mechanical balance of the cluster. It can be seen as a zero net force over the boundary Γ_C.

- Edges close to the hole cannot be considered as free edges as argued in Section 3.3.2. Yet, the missing matter should be balanced and this case can be treated as previously: a zero net force over the boundary $\tilde{\Gamma}_H$ can be written, similarly than in Eq. (12).

In the case of $\tilde{\Gamma}_B$, there is no need to evaluate the stress at these nodes. Indeed, the global balance brings the stress response with the neighbour nodes in the bulk. A similar way to deal with the boundary consists in treating it as $\tilde{\Gamma}_T$.

3.3.4 Graphical summary of the practical challenges

Figure 5 summarizes our solutions to the practical challenges.

Finally, the minimisation process consists in finding the stress closest to the material states under the constraints of mechanical equilibrium (as described in 2.2: step 2 of the algorithm). The constraints are enforced in the algorithm at each nodes for the bulk (Eq. (9)) and as a net force over all nodes of the concerned boundary Γ: $\sum_{j\in\Gamma} f_j = F_\Gamma$ (with f_j the mechanical stress contribution at the node j, *i.e.* the nodal force). The force input F over Γ is the net force over the top boundary (in the sensor direction) (Eq. (11)), and is null over the cluster or holes boundaries (Eq. (12)).

4 Results and discussion

For the experiments described in Section 3.1, the above-mentionned methods of correction are applied to data issued from DIC; then the DDI algorithm is applied.

4.1 Parameters and computation

For the DDI algorithm, the following intrinsic parameters are adopted.

- The number of images, which is here the number of loading increments, is $N_Y = 165$. Thanks to this sufficiently large number of images, the displacement fields measured by DIC do not exhibit too much missing data. Considering that the DIC process yields meshes with about $8 \cdot 10^5$ nodes and $N_{\text{elem}} \approx 1.6 \cdot 10^5$ linear triangular elements, the total number of computed mechanical states is $N_{\text{mecha}} = N_{\text{elem}} \times N_Y \approx 2.7 \cdot 10^7$.

- The number of material states, which sample the material response, is chosen accordingly to the total number of computed mechanical states: $N^* = \frac{N_{\text{mecha}}}{100} \approx 2.7 \cdot 10^5$. From a practical point of view, initial values of the material states are computed thanks to the *k-means* method. The choice of the number of material states N^* is also of importance as it changes the mapping between mechanical and material states and so the convergence of the method. A too small number of material states allows the mechanical states (stress in particular) to be far from their associated material state, it adds freedom when solving the algorithm but implies large error. Conversely, a too large number constrains the mechanical stresses to be close to their material data point and the algorithm can stop on local minima. Our previous works on synthetic data suggest one material states every 100 mechanical states.

- The tensor $\mathbb{C}$ of the norm Eq. (7) is chosen as:

$$\mathbb{C} = C \cdot \mathbb{I} \tag{13}$$

  where $C = 10^{10}$ Pa and $\mathbb{I}$ the fourth-order identity tensor.

Computations are carried out with Matlab on a single machine with 24 cores. Computation time is about 40 h. No particular care has been taken to explicitly parallelize the algorithm. We recall here that the outputs are twofold: all the mechanical states and a database of material states, respectively referred to as (O-1) and (O-2) in Section 2.1.

4.2 Measurement of heterogeneous stress fields

First, we focus on the first output (O-1) of the DDI algorithm: the stress field σ_e^Y for each mechanical problem. Figure 6 presents the three in-plane components of the stress field for a given mechanical problem Y.

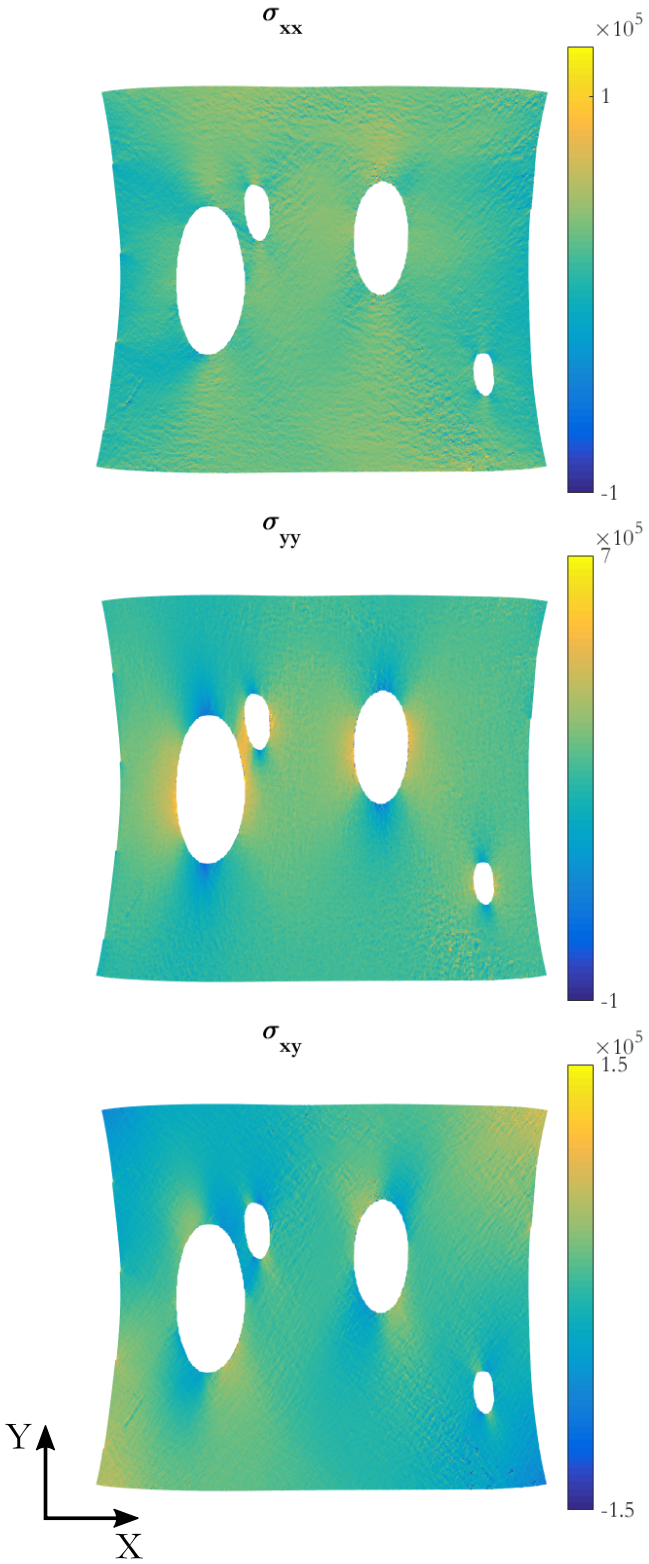

Figure 6: Components of the stress field computed by the DDI algorithm for one mechanical problem.

Both spatial distribution and order of magnitude of the stress field are relevant. As example, the stress component in the tensile direction σ_{yy} is maximum close to holes highlighting stress concentration and reveals compressive states at top and bottom of these holes. The transversal stress σ_{xx} is noisier: displacements in the x-direction are very small and they lead to insufficiently rich inputs for the DDI algorithm (input (I-1) in Section 2.1) . Moreover, only one mechanical problem is shown; on others, we could observe some white spots in stress distributions: they correspond to clusters of missing data.

4.3 Relevance of the results

Discussing the validity of the present approach is not an easy task. Indeed, the naive approach would consist in fitting a hyperelastic constitutive equation, *e.g.* Mooney-Rivlin or Ogden models, thanks to uniaxial tensile experimental data and comparing stress fields issued from the DDI method with those obtained with Finite Element computations. Nevertheless, such an approach presupposes that numerical results issued from a chosen constitutive model are more valid than the ones measured here.

This is not our point of view: we prefer to discuss the results by examining if measured stress fields respect some features of the material response. More precisely, the following questions are investigated: is the isotropy of the material recovered? is its uniaxial tensile response retrieved? In the following, material states (output (O-2)) are used to answer the former question and all measured mechanical states (output (O-1)) to answer the latter one by considering the strain energy density.

4.3.1 Isotropy of the material

The material itself and the moulding process employed for the sample ensure that its mechanical response is isotropic. In the DDI method, material states, *i.e.* stress-strain couples, are computed with no reference to material symmetry. To verify if measured material states recover isotropy, the misalignment angle between the eigenvectors of strain and stress tensors corresponding to their respective largest principal value is computed for all N^* material states. The corresponding results are shown in Figure 7. For more than 90%, respectively 60%, this misalignment is less than $\pm 10.8^\circ$, respectively $\pm 4.6^\circ$. So, using real data, the isotropy of the material is retrieved by the DDI algorithm.

4.3.2 Strain energy density

We consider the uniaxial deformation from the undeformed initial state to a given final mechanical problem Y. This process is parametrized by the time τ such that $\tau = 0$ initially and $\tau = t$ for the problem Y. For a given quadrature point defined

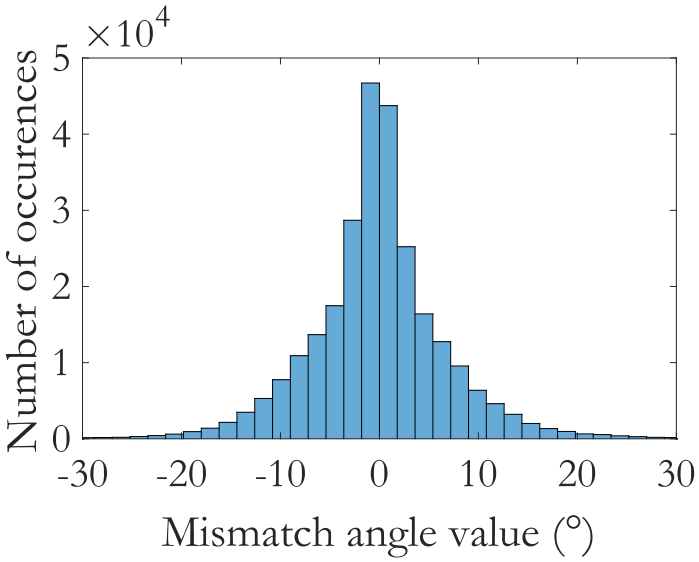

Figure 7: Histogram of misalignment angle between principal stress and strain of the material database.

by its initial position $\mathbf{X}$ (in the case of linear triangles, it is the centre of the corresponding finite element) at time $\tau = 0$ and its spatial position $\mathbf{x}(\mathbf{X},\tau)$ in one of the state in $[0,t]$ the stress power density p_{int} is defined by [26]:

$$p_{\text{int}}(\mathbf{x},\tau) = \boldsymbol{\sigma}(\mathbf{x},\tau) : \mathbf{d}(\mathbf{x},\tau) \tag{14}$$

where $\boldsymbol{\sigma}(\mathbf{x},\tau)$ is the stress tensor measured by DDI and $\mathbf{d}(\mathbf{x},\tau)$ is the rate of deformation tensor that can be derived from DIC measurements.

Considering now the whole tensile test from 0 to t, the corresponding strain energy density for a given point $\mathbf{X}$ is:

$$w(\mathbf{x}(\mathbf{X},t),t) = \int_0^t p_{\text{int}}(\mathbf{x}(\mathbf{X},\tau),\tau)\,\mathrm{d}\tau. \tag{15}$$

By definition, this strain energy is defined per unit of deformed volume. In order to recover the standard strain energy density $W(\mathbf{X},\tau)$ defined per unit undeformed volume, we simply invoke the incompressibility of the material such that

$$W(\mathbf{X},t) = w(\mathbf{x}(\mathbf{X},t),t). \tag{16}$$

In the classical isotropic incompressible hyperelasticity theory, the strain energy density is revealed to be a function of the two first strain invariants defined by:

$$I_1 = \mathrm{tr}(\mathbf{b}) \quad \text{and} \quad I_2 = \frac{1}{2}\left[\mathrm{tr}(\mathbf{b})^2 - \mathrm{tr}(\mathbf{b}^2)\right], \tag{17}$$

the third strain invariant $\det(\mathbf{b})$ being equal to 1 due to incompressibility. These two invariants are computed for each point $\mathbf{X}$ and time t. Figure 8 presents the

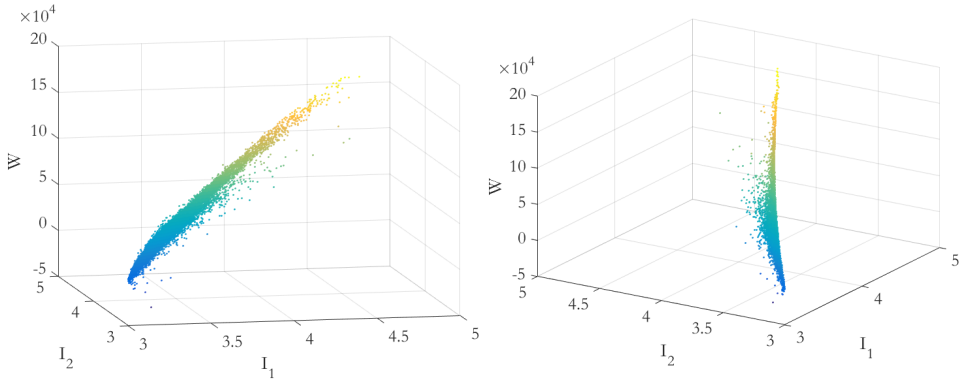

Figure 8: Strain energy density measured by DDI for inhomogeneous experiments with respect to the two first strain invariants.

strain energy density $W(\mathbf{X},t)$ of all mechanical states, *i.e.* all elements defined by $\mathbf{X}$ for all mechanical problems, obtained using DDI, as a function of these strain invariants.

Finally, the ability to compute the strain energy density can be considered to fit classical hyperelastic models or to use model-free methods such as the *What-You-Prescribed-is-What-You-Get (WYPiWYG)* method [14].

Remark. In the incompressible framework, the stress field consists in a "material" contribution $\overline{\sigma}$ and a "structural" one defined by a hydrostatic pressure p which acts as a Lagrange multiplier of the incompressibility condition:

$$\sigma = \overline{\sigma} - p\mathbf{I}, \tag{18}$$

$\mathbf{I}$ being the 3×3 identity tensor. As p depends on the mechanical problem, the stress field σ shown in Fig. 6 does not represent completely the mechanical response of the material. This limitation has been overcome thanks to the strain energy density. Indeed, as the incompressibility constraint can be written as $\mathrm{tr}(\mathbf{d}) = 0$, the stress power density Eq. (14) reduces to

$$p_{\mathrm{int}} = \overline{\sigma} : \mathbf{d}. \tag{19}$$

Thus, the strain energy density issued from Eqs ((15)-(16)) describes only the material response.

In order to further discuss our results, we plot the Uniaxial Tensile (UT) strain energy obtained with classical uniaxial tensile tests in Figure 9. At small strain, the accordance is good, but at larger strain, one can observe a mismatch. It is believed that the discrepancy between strain energies from DDI and UT is mainly due to the error on thickness measurement e_0 [32]. For both experiments, the thickness is supposed to be given at $\pm\Delta e_0 = \pm$ 0.7mm. This uncertainty is also plotted on the Figure and for graphical clarity both are reported on the uniaxial curve with $2\Delta e_0 = 1.4$ mm.

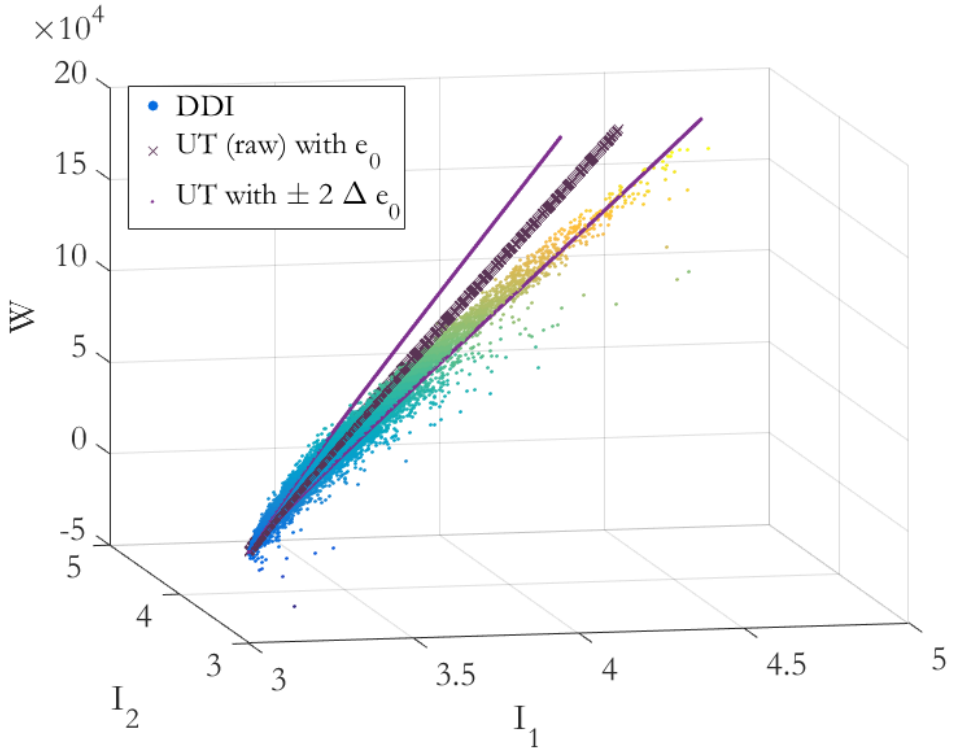

Figure 9: Strain energy densities from the DDI procedure and from uniaxial tensile test, with respect to the two first strain invariants, with uncertainty of thickness measurement.

5 Conclusion

In this paper, an original coupled experimental-numerical method has been proposed to measure heterogeneous stress fields. Indeed, mixing DIC measurements with the recent Data Driven Identification algorithm allows one to determine the stress field in a complex sample without prescribing any constitutive equation. As a proof of concept, the method has been applied to a multi-perforated elastomer membrane under uniaxial loading conditions. Practical challenges regarding missing data in measured displacement fields and nodal forces have been addressed. DDI algorithm outputs are twofold. First, the mechanical states consisting in heterogeneous stress and strain fields that exactly satisfy equilibrium equations and boundary conditions are derived. Then, the method is revealed able to determine the heterogeneous stress distribution on a planar complex sample using the kinematic DIC measurements. Second, the database of material states that samples the material response is build. Such database is actually the missing piece to the work of Ortiz *et al.* [16] or Ibañez [33] to perform mechanical simulation without constitutive equation. Mechanical and material states are relevant, both qualitatively and quantitatively, when compared to classical uniaxial testing data of the material. Further work is in progress to challenge the method with more complex problems: larger strain, heterogeneous materials, multiaxial loading conditions and inelasticity.

Acknowledgements This work was performed by using HPC resources of Centrale Nantes Supercomputing Center on the cluster Liger, granted and identified D1705030 by the High Performance Computing Institute (ICI).

References

References

[1] G. Marckmann, E. Verron, Comparison of Hyperelastic Models for Rubber-Like Materials, Rubber Chemistry and Technology 79 (5) (2006) 835–858. doi:10.5254/1.3547969.
URL http://rubberchemtechnol.org/doi/abs/10.5254/1.3547969

[2] M. A. Sutton, J. J. Orteu, H. Schreier, Image Correlation for Shape, Motion and Deformation Measurements: Basic Concepts,Theory and Applications, Springer Science & Business Media, 2009.

[3] S. Avril, M. Bonnet, A.-S. Bretelle, M. Grédiac, F. Hild, P. Ienny, F. Latourte, D. Lemosse, S. Pagano, E. Pagnacco, F. Pierron, Overview of Identification Methods of Mechanical Parameters Based on Full-field Measurements, Experimental Mechanics 48 (4) (2008) 381. doi:10.1007/s11340-008-9148-y.

URL https://link.springer.com/article/10.1007/s11340-008-9148-y

[4] M. Grédiac, F. Pierron, S. Avril, E. Toussaint, The Virtual Fields Method for Extracting Constitutive Parameters From Full-Field Measurements: a Review, Strain 42 (4) (2006) 233–253. doi:10.1111/j.1475-1305.2006.tb01504.x.
URL https://onlinelibrary.wiley.com/doi/abs/10.1111/j.1475-1305.2006.tb01504.x

[5] M. J. Berry, G. Linoff, Data Mining Techniques: For Marketing, Sales, and Customer Support, John Wiley & Sons, Inc., New York, NY, USA, 1997.

[6] J. Ling, R. Jones, J. Templeton, Machine learning strategies for systems with invariance properties, Journal of Computational Physics 318 (2016) 22–35. doi:10.1016/j.jcp.2016.05.003.
URL http://www.sciencedirect.com/science/article/pii/S0021999116301309

[7] Y. Shen, K. Chandrashekhara, W. F. Breig, L. R. Oliver, Finite element analysis of V-ribbed belts using neural network based hyperelastic material model, International Journal of Non-Linear Mechanics 40 (6) (2005) 875–890. doi:10.1016/j.ijnonlinmec.2004.10.005.
URL http://www.sciencedirect.com/science/article/pii/S0020746204001635

[8] T. Furukawa, G. Yagawa, Implicit constitutive modelling for viscoplasticity using neural networks, International Journal for Numerical Methods in Engineering 43 (2) (1998) 195–219. doi:10.1002/(SICI)1097-0207(19980930)43:2<195::AID-NME418>3.0.CO;2-6.
URL https://onlinelibrary.wiley.com/doi/abs/10.1002/%28SICI%291097-0207%2819980930%2943%3A2%3C195%3A%3AAID-NME418%3E3.0.CO%3B2-6

[9] Y. M. A. Hashash, S. Jung, J. Ghaboussi, Numerical implementation of a neural network based material model in finite element analysis, International Journal for Numerical Methods in Engineering 59 (7) (2004) 989–1005. doi:10.1002/nme.905.
URL https://onlinelibrary.wiley.com/doi/abs/10.1002/nme.905

[10] L. Meng, P. Breitkopf, B. Raghavan, G. Mauvoisin, O. Bartier, X. Hernot, Identification of material properties using indentation test and shape manifold learning approach, Computer Methods in Applied Mechanics and Engineering 297 (2015) 239–257. doi:10.1016/j.cma.2015.09.004.
URL http://linkinghub.elsevier.com/retrieve/pii/S0045782515002984

[11] D. Millán, M. Arroyo, Nonlinear manifold learning for model reduction in finite elastodynamics, Computer Methods in Applied Mechanics and Engineering 261–262 (2013) 118–131. doi:10.1016/j.cma.2013.04.007.
URL http://www.sciencedirect.com/science/article/pii/S0045782513001059

[12] J. Réthoré, A. Leygue, M. Coret, L. Stainier, E. Verron, Computational measurements of stress fields from digital images, International Journal for Numerical Methods in Engineering 113 (12) (2018) 1810–1826. doi:10.1002/nme.5721.
URL https://onlinelibrary.wiley.com/doi/abs/10.1002/nme.5721

[13] R. Seghir, F. Pierron, A Novel Image-based Ultrasonic Test to Map Material Mechanical Properties at High Strain-rates, Experimental Mechanics 58 (2) (2018) 183–206. doi:10.1007/s11340-017-0329-4.
URL https://doi.org/10.1007/s11340-017-0329-4

[14] M. Latorre, F. J. Montáns, Experimental data reduction for hyperelasticity, Computers & Structuresdoi:10.1016/j.compstruc.2018.02.011.
URL http://www.sciencedirect.com/science/article/pii/S0045794917306259

[15] A. Leygue, M. Coret, J. Réthoré, L. Stainier, E. Verron, Data-based derivation of material response, Computer Methods in Applied Mechanics and Engineering 331 (2018) 184–196. doi:10.1016/j.cma.2017.11.013.
URL http://www.sciencedirect.com/science/article/pii/S0045782517307156

[16] T. Kirchdoerfer, M. Ortiz, Data-driven computational mechanics, Computer Methods in Applied Mechanics and Engineering 304 (2016) 81–101. doi:10.1016/j.cma.2016.02.001.
URL http://www.sciencedirect.com/science/article/pii/S0045782516300238

[17] T. Kirchdoerfer, M. Ortiz, Data Driven Computing with noisy material data sets, Computer Methods in Applied Mechanics and Engineering 326 (2017) 622–641. doi:10.1016/j.cma.2017.07.039.
URL http://www.sciencedirect.com/science/article/pii/S0045782517304012

[18] L. T. K. Nguyen, M.-A. Keip, A data-driven approach to nonlinear elasticity, Computers & Structures 194 (2018) 97–115. doi:10.1016/j.compstruc.2017.07.031.
URL http://www.sciencedirect.com/science/article/pii/S0045794917301311

[19] T. Kirchdoerfer, M. Ortiz, Data-driven computing in dynamics, International Journal for Numerical Methods in Engineering 113 (11) (2018) 1697–1710. doi:10.1002/nme.5716.

[20] J. Ayensa-Jiménez, M. H. Doweidar, J. A. Sanz-Herrera, M. Doblaré, A new reliability-based data-driven approach for noisy experimental data with physical constraints, Computer Methods in Applied Mechanics and Engineering 328 (2018) 752–774. doi:10.1016/j.cma.2017.08.027.
URL http://www.sciencedirect.com/science/article/pii/S0045782517304255

[21] Y. Kanno, Mixed-Integer Programming Formulation of a Data-Driven Solver in Computational Elasticity.
URL https://arxiv.org/abs/1810.04394

[22] J. MacQueen, others, Some methods for classification and analysis of multivariate observations, in: Proceedings of the fifth Berkeley symposium on mathematical statistics and probability, Vol. 1, Oakland, CA, USA, 1967, pp. 281–297.

[23] L. Meunier, G. Chagnon, D. Favier, L. Orgéas, P. Vacher, Mechanical experimental characterisation and numerical modelling of an unfilled silicone rubber, Polymer Testing 27 (6) (2008) 765–777. doi:10.1016/j.polymertesting.2008.05.011.
URL http://www.sciencedirect.com/science/article/pii/S0142941808000986

[24] M. A. Sutton, J. H. Yan, V. Tiwari, H. W. Schreier, J. J. Orteu, The effect of out-of-plane motion on 2d and 3d digital image correlation measurements, Optics and Lasers in Engineering 46 (10) (2008) 746–757. doi:10.1016/j.optlaseng.2008.05.005.
URL http://www.sciencedirect.com/science/article/pii/S0143816608000985

[25] E. Jones, M. E. Iadicola, A Good Practices Guide for Digital Image Correlation, Tech. rep., International Digital Image Correlation Society (2018). doi:10.32720/idics/gpg.ed1.
URL http://idics.org/guide/

[26] G. A. Holzapfel, Nonlinear Solid Mechanics, John Wiley & Sons, 2000.

[27] R. Eggersmann, T. Kirchdoerfer, S. Reese, L. Stainier, M. Ortiz, Model-Free Data-Driven inelasticity, Computer Methods in Applied Mechanics and Engineering 350 (2019) 81–99. doi:10.1016/j.cma.2019.02.016.
URL http://www.sciencedirect.com/science/article/pii/S0045782519300878

[28] A. Leygue, R. Seghir, J. Réthoré, M. Coret, E. Verron, L. Stainier, Non-parametric material state field extraction from full field measurements, Computational Mechanics (2019) 1–9doi:10.1007/s00466-019-01725-z.
URL https://doi.org/10.1007/s00466-019-01725-z

[29] M. Dalemat, M. Coret, A. Leygue, E. Verron, Reliability of the Data-Driven Identification algorithm with respect to incomplete input data, in: The European Conference on Constitutive Models for Rubber 2019, Nantes, France, 2019.

[30] F. Hild, S. Roux, Comparison of Local and Global Approaches to Digital Image Correlation, Experimental Mechanics 52 (9) (2012) 1503–1519. doi:10.1007/s11340-012-9603-7.
URL https://doi.org/10.1007/s11340-012-9603-7

[31] J. Réthoré, T. Elguedj, M. Coret, P. Chaudet, A. Combescure, others, Robust identification of elasto-plastic constitutive law parameters from digital images using 3d kinematics, International Journal of Solids and Structures 50 (1) (2013) 73–85.
URL http://www.sciencedirect.com/science/article/pii/S0020768312003836

[32] S. A. O'Leary, B. J. Doyle, T. M. McGloughlin, Comparison of methods used to measure the thickness of soft tissues and their influence on the evaluation of tensile stress, Journal of Biomechanics 46 (11) (2013) 1955–1960. doi:10.1016/j.jbiomech.2013.05.003.
URL http://www.sciencedirect.com/science/article/pii/S0021929013002248

[33] R. Ibáñez Pinillo, E. Abisset-Chavanne, J. V. Aguado, D. González, E. Cueto, F. Chinesta, A manifold learning approach to data-driven computational elasticity and inelasticity, Archives of Computational Methods in Engineering 25. doi:10.1007/s11831-016-9197-9.